Original Article

Avicenna Journal of Medical Biotechnology
Volume 18, Issue 1, 79-93
https://doi.org/10.18502/ajmb.v18i1.21052

Check for updates

In vitro and *In silico* Analysis of *SCIN* rs376349889 as a Potential Biomarker for Gastric and Colorectal Cancers

Neda Vaghefinezhad [1], Mansoureh Azadeh [2], Majid Tafrihi [1*] and Abasalt Hosseinzadeh Colagar [1]

1. Department of Molecular and Cell Biology, Faculty of Basic Sciences, University of Mazandaran, Babolsar, Mazandaran, Iran
2. Zist-Fanavari Novin Biotechnology Institute, Isfahan, Iran

*** Corresponding author:**
Majid Tafrihi, Ph.D., Department of Molecular and Cell Biology, Faculty of Basic Sciences, University of Mazandaran, Babolsar, Mazandaran, Iran
Tel: +98 1135305252
Fax: +98 1135302450
E-mail: m.tafrihi@umz.ac.ir
Received: 9 Jun 2025
Accepted: 17 Oct 2025

Abstract

Background: Numerous research endeavors have reported altered expression of Scinderin (*SCIN*) in various cancer types. Single Nucleotide Polymorphisms (SNPs) represent the most prevalent form of genetic variation within the human genome which can have significant functional consequences, including cancer predisposition.

Methods: This study investigated SNP-induced structural alterations in the SCIN protein and their potential effects on stability and function, using *in vitro* and *in silico* approaches. Integrating experimental and computational data provides insight into the role of this variant in tumorigenesis and highlights its potential as a molecular biomarker for cancer diagnosis and prognosis.

Results: Out of 1,054 nonsynonymous SNPs (nsSNPs), 11 were consistently predicted to be deleterious. Among them, rs376349889 (R511G) was associated with decreased protein stability, loss of ADP-ribosylation at R511, disrupted ionic interactions, and increased hydrophobicity, all of which may impair SCIN function. Subsequently, genotyping of 200 colorectal cancer and 200 gastric cancer samples for the rs376349889 SNP was performed using High-Resolution Melting (HRM) technique in compared to a matched control group.

Conclusion: The findings revealed a considerable difference in the allelic prevalence of the rs376349889 SNP between cancer patients and control samples. Notably, the GG genotype was linked to a higher susceptibility to both gastric and colorectal cancers ($p<0.0001$). These results suggest that rs376349889 may influence *SCIN*-related oncogenic mechanisms and could serve as a promising biomarker for identifying or evaluating the risk of gastrointestinal cancers at an early stage.

Keywords: Biomarkers, Colorectal neoplasm, Gastric neoplasm, Scinderin, Single nucleotide polymorphism
To cite this article: Vaghefinezhad N, Azadeh M, Tafrihi M, Hosseinzadeh Colagar A. *In vitro* and *In silico* Analysis of *SCIN* rs376349889 as a Potential Biomarker for Gastric and Colorectal Cancers. Avicenna J Med Biotech 2026;18(1):79-93.

Introduction

Gastric Cancer (GC) is one of the most frequently diagnosed and difficult-to-treat cancers, globally. This complex disease varies significantly from person to person, with each case often displaying unique genetic and molecular characteristics. Such individuality highlights the intricate nature of GC and the need for personalized approaches to treatment [1]. Gastric cancer poses a significant health burden, worldwide, ranking as the fifth among cancers (accounting for 5.6% of cases) and the third leading cause of cancer-related deaths (7.7%) [2,3].

Colorectal Cancer (CRC) ranks third in global cancer incidence and is the second most frequent cause of cancer-related mortality [4]. The overwhelming majority of CRC cases fall under the category of "sporadic," denoting the absence of any recognizable hereditary syndromes, with only a small fraction (2-8%) attributed to hereditary factors [5]. Colorectal cancer is believed to develop due to a combination of inherited genes, environmental factors, and lifestyle [6].

Scinderin (SCIN), a protein named after the Latin term "scindere" meaning "to cut," functions as a Ca^{2+}-dependent regulator of actin filament breakdown, belonging to the gelsolin superfamily [7]. Its involvement

extends to various physiological conditions such as exocytosis, megakaryopoiesis, autoimmune conditions, and tumorigenesis. Through the modulation of F-actin dynamics, Scinderin orchestrates the translocation of secretory vesicles and impacts cell migration by governing the process of Epithelial-Mesenchymal Transition (EMT) [8,9].

Single Nucleotide Polymorphisms (SNPs) represent one of the major forms of genetic variation within the human genome that is correlated with an individual's genetic predisposition to cancer [10-12]. SNPs located in coding regions include synonymous and non-synonymous mutations that synonymous mutations have the potential to influence the expression of the protein by modulating post-transcriptional modifications, translation rates, and various additional processes. Conversely, non-synonymous SNPs (nsSNPs) induce alterations in the protein structure, as well as its physical and chemical attributes, including stability and solubility, thereby affecting its functionality [13].

Investigating genes containing SNPs contributes significantly to early cancer detection and the customization of therapies. To date, no functional investigations have explored the impact of *SCIN* polymorphisms on gene regulation or functionality in gastrointestinal cancer.

The present study aimed to evaluate a SNP in the *SCIN* gene as a potential biomarker for cancer. To this end, a combination of *in vitro* and *in silico* approaches was employed to assess the potential effects of this genetic variation on structural stability, and protein function. For this investigation, focus was made on two cancers, GC and CRC, selected due to their physiological and anatomical similarity, which facilitates comparative analysis and may reveal shared molecular mechanisms underlying tumor development. For this purpose, the HRM method was applied to evaluate the correlation between SNP rs376349889 and the susceptibility to GC and CRC. The methodology employed in the current study is briefly demonstrated figure 1. This study represents the first comprehensive investigation of the functional and structural nsSNPs within the Scinderin protein, utilizing both *in silico* and *in vitro* approaches. Nonetheless, further clinical research involving diverse ethnic groups is warranted to confirm these results.

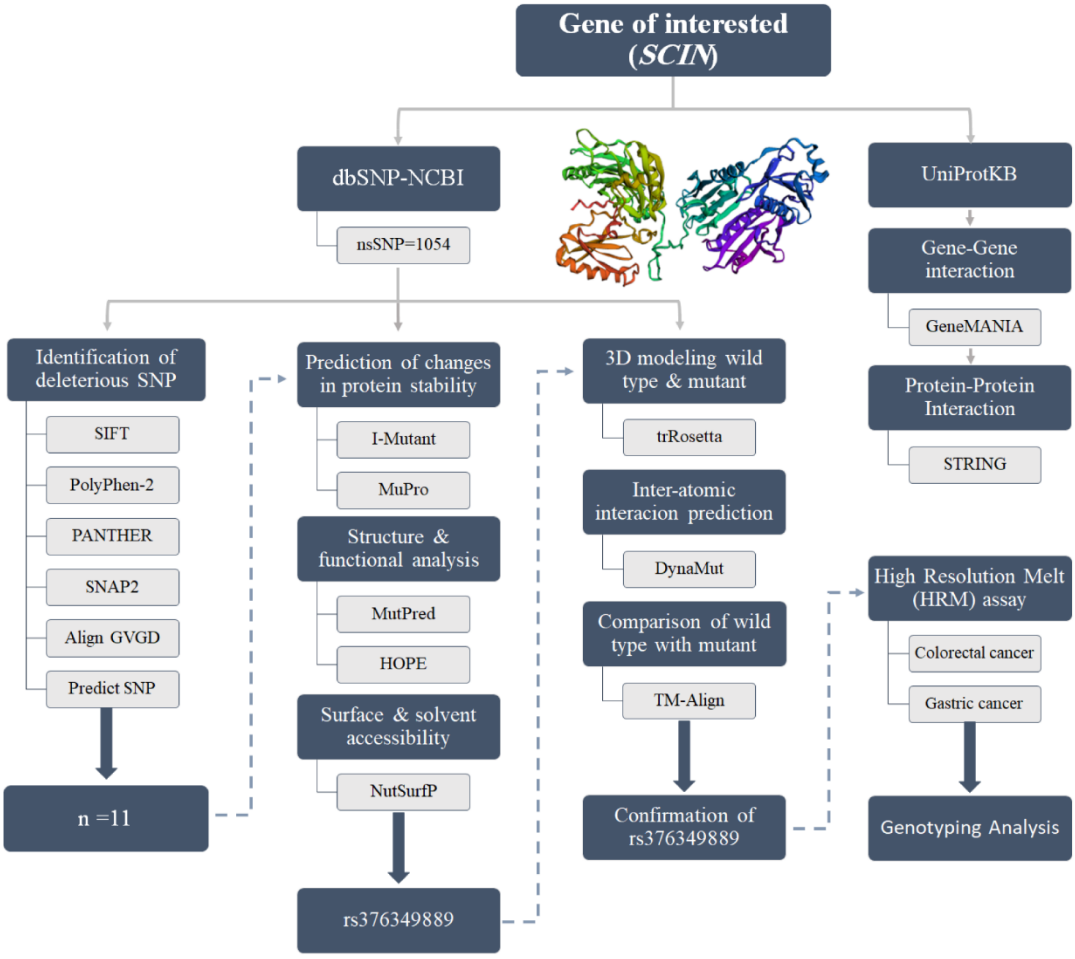

Figure 1. Flowchart outlining the steps taken to identify the rs376349889 SNP and the associated experimental designs. Integration of *In vitro* and *In silico* analyses to identify functionally significant SNPs, evaluate their effects on protein structure and stability, analyze their roles in gene-gene and protein-protein interaction networks, and ultimately identify potential molecular biomarkers for disease diagnosis, prognosis, or therapeutic applications.

Materials and Methods

Scinderin protein profiling and retrieval of SNP data

To gather information on the *SCIN* gene (UniProt ID: Q9Y6U3), including the amino acid sequence and functional attributes, we accessed the UniProtKB database (http://www.uniprot.org/uniprot/). For a deeper understanding of the Scinderin protein, InterPro database (https://www.ebi.ac.uk/interpro/), was utilized which helps to identify specific domains, motifs, and other conserved features. This allowed the authors to explore the protein's structure and potential functions by referencing a comprehensive collection of protein families and functional site data [14].

Additionally, Scinderin structural property prediction was performed using RaptorX property, a web server that predicts structural properties of protein sequences without relying on a template (http://raptorx6.uchicago.edu/StructurePropertyPred/predict/) [15].

The data regarding SNPs of the human *SCIN* gene were acquired from the dbSNP-NCBI database (http://www.ncbi.nlm.nih.gov/SNP/). Subsequently, the nsSNPs were excluded to facilitate further investigations [16].

Identification of potentially deleterious SNP variants

To assess the potential impact of SNPs in the *SCIN* gene's coding sequence, multiple bioinformatic platforms—SIFT, PANTHER, PolyPhen-2, SNAP2, PredictSNP, and Align GVGD were employed.

Analyzing potential deleterious effects of nsSNPs was conducted using the Sorting Intolerant from Tolerant (SIFT) web-based tool (http://sift.jcvi.org/). SIFT evaluates the impact of each SNP by considering both sequence similarity and the physical properties of the protein. The SIFT scores ranged from 0 to 1, where a score lower than 0.05 suggests the adverse influence of nsSNPs on protein structure or function [17].

The PolyPhen-2 tool (http://genetics.bwh.harvard.edu/pph2) evaluates how changes in amino acids influence protein structure and functions through sequence-based characterization. Predictions were given as probability values divided into three distinct groups: "benign", "possibly damaging", and "probably damaging" with a cutoff value that has been set for probably damaging, with a score exceeding 0.95 [18].

The PANTHER-PSEP web server (http://pantherdb.org/tools/csnpScoreForm.jsp) categorizes the impact of nsSNPs on protein activity by considering evolutionary relationships, molecular functions, and protein-protein interactions. It examines amino acid changes through evolutionary conservation scores obtained from aligned sequences of diverse, related proteins [19].

The SNAP2 web server (https://www.rostlab.org/services/SNAP/) relies on neural network algorithms to make predictions regarding the influence of nsSNPs on secondary structure of proteins. Additionally, a solvent accessibility comparison is performed between the native and altered protein structures to help separate functionally relevant changes from neutral ones [20].

The Align GVGD online tool (http://agvgd.hci.utah.edu/) is grounded in biophysical characterization. By integrating multiple sequence alignments of proteins with amino acid biophysical characteristics, this tool effectively forecasts the impact of a missense change as either benign or harmful. These mutations are classified into seven groups: C0, considered the most probable to be neutral or benign, C15, C25, C35, C45, C55, and C65, identified as the most likely to be deleterious or pathogenic [21].

The PredictSNP online tool (https://loschmidt.chemi.muni.cz/predictsnp1/) compiles data inputs from multiple sources to determine the potential impact of amino acid changes. By adopting this collaborative approach, PredictSNP offers a more comprehensive view and improves predictive accuracy compared to individual predictors [22].

Different tools use various algorithms, so single nucleotide polymorphisms identified by all of them as having harmful effects-such as changes in structural stability, energy levels, and surface availability-were selected for further analysis.

Assessment of structural stability alterations in mutant proteins

Protein function is linked to its stability, emphasizing the importance of identifying alterations in protein stability caused by nsSNPs. Five computational tools—IMutant2.0, MutPred2, MUpro, NetSurfP-2.0, and HOPE—were employed to evaluate the stability of the mutated protein.

IMutant2.0 (http://folding.biofold.org/i-mutant/imutant2.0.html) is an SVM-based tool used to assess whether a modification in an amino acid affects protein stability. The analysis of nsSNPs using this tool was conducted under specific conditions: a temperature of 25°*C* and a pH of 7.0, while relying on the ΔΔG value and binary classification system for the prediction process. The assessment relies on ΔΔG values, reflecting the difference in Gibbs free energy between the wild-type and mutated forms. Additionally, an RI value, denoting the reliability index, was assigned to each result generated by the tool. A ΔΔG value below 0 indicates reduced protein stability, whereas a value above 0 signifies increased stability [23].

MUpro (http://mupro.proteomics.ics.uci.edu/) is a web-based tool is utilized to predict protein stability alterations caused by SNPs, employing Support Vector Machine (SVM) and neural networks algorithms. Stability predictions can be made using this tool without the need for tertiary structure input. The results indicate the energy variation due to an amino acid substitution, presented as a ΔΔG value with a confidence rating from -1 to 1. A ΔΔG value below 0, signifies reduced protein stability, while a value above 0 indicates increased stability [24].

To evaluate the predicted structural and functional consequences of amino acid substitutions, the MutPred2 server (http://mutpred.mutdb.org/) was utilized.

Amino acid modifications can affect protein functionality in various ways, including structural destabilization, disruption of macromolecular binding, and loss of Post-Translational Modifications (PTM) sites. These alterations in molecular processes often play a significant role in modifying the phenotypic effects of a protein. Using the MutPred2 algorithm, SNP pathogenicity levels are assessed, and a wide range of structural and functional modifications resulting from these amino acid changes are predicted. Additionally, empirical p-values are provided for each modification [25].

To predict the secondary structure and exposure level of amino acids on the protein surface, the NetSurfP server (http://www.cbs.dtu.dk/services/NetSurfP/) was employed. Using a neural network-based architecture that integrates convolutional and long short-term memory networks, this tool analyzes the amino acid sequence to predict exposure level of amino acids on the protein surface, secondary structure, and structural changes at each position. The Relative Surface Accessibility (RSA) threshold is set at 25%; residues with RSA >25% are classified as exposed [26].

The HOPE server (https://www3.cmbi.umcn.nl/hope/) was employed to assess the impact of deleterious SNPs on the three-dimensional protein structure. HOPE provides insights into how SNPs affect properties such as residue size, electrical charge, hydrophobicity, spatial conformation, bond alterations, and functional characteristics, with integrated 3D visualization. Additionally, HOPE evaluates the conservation score of the altered residue using HSSP multiple-sequence alignment [27].

Protein modelling and structural analysis

Both the wild-type and mutant proteins, which exhibited a significant impact following a point mutation based on initial analysis, were modeled using the trRosetta algorithm. This online tool predicts the structural arrangement of proteins (https://yanglab.nankai.edu.cn/trRosetta/) through a deep learning-based *ab initio* folding approach [28].

The mutated models were evaluated using the TM-align tool (https://zhanglab.dcmb.med.umich.edu/TM-align/) to assess structural deviations between the native and mutant models. TM scores and Root Mean Square Deviation (RMSD) values were computed by superimposing the protein structures to identify structural similarities. TM scores range from 0 to 1, with a value of 1 signifies a a perfect structural match. A TM score between 0.0 and 0.30 suggests random structural similarity, whereas a score of 0.5 or higher indicates that the structures share the same fold [29].

Computational analysis of nsSNP-induced changes in protein stability and interactions

The DynaMut server (http://biosig.unimelb.edu.au/dynamut/) was employed to predict how nsSNPs influence protein stability and molecular interactions. This server predicts structural changes by analyzing protein flexibility and dynamics. DynaMut utilizes Normal Mode Analysis (NMA) to calculate the difference in Gibbs free energy (ΔΔG) between the Wild-Type (WT) and Mutant (MT) protein structures. It also evaluates the change in flexibility ENCoM-based vibrational entropy differences (ΔΔSVib). DynaMut further provides insights into how mutations affect protein conformation, flexibility, and stability, along with visualizations of dynamic behavior [30].

Gene-gene interaction analysis

The potential associations among gene networks and gene interactions were predicted using the GeneMANIA online tool (http://genemania.org/). This information includes gene-gene and protein-protein interactions, structural resemblance of protein domains, co-expression, pathways, and colocalization. When given a list of query genes, GeneMANIA expands this list by incorporating functionally similar genes based on available genomics and proteomics data. The gene of interest was analyzed using GeneMANIA to visualize and explain the interconnections among the identified genes [31].

Protein-protein interaction (PPI) network analysis

Amino acid sequence alteration can lead to conformational changes in proteins, potentially affecting their functional properties. As a result, the mutated protein may interact with different partners, resulting in observable phenotypic effects. To explore the interaction patterns of SCIN with various proteins, the STRING server (http://string-db.org/) was utilized. This platform offers a comprehensive analysis of protein-protein interactions, incorporating both predicted and experimentally validated interactions [32].

Sample preparation

The study population comprised 200 GC patients, 200 CRC patients, and 200 healthy controls. Blood samples were collected from all participants—following informed consent at Sayed-Al-Shohada and Al-Zahra hospitals in Isfahan, Iran. Approximately 5 *ml* of peripheral blood was drawn from all enrolled individuals and collected in tubes containing EDTA as an anticoagulant. Genomic DNA was isolated using the GeneAll Exgene kit (Korea) in accordance with the manufacturer's protocol.

Real-time PCR and high-resolution melting (HRM) analysis

The sequence of SNP rs376349889 was identified using the GeneBank database. The sequence and additional information related to this SNP were obtained from NCBI. The online tool Primer3Plus (https://www.bioinformatics.nl/cgi-bin/primer3plus/primer3plus.cgi) was used to design a specific pair of primers. Primer melting temperatures (Tm) and design suitability parameters were assessed using OligoAnalyzer, and primer specificity was assessed using the Primer-BLAST online tool (https://www.ncbi.nlm.nih.gov/tools/primer-blast/).

The HRM technique was employed for amplifica-

tion reactions using a MIC qPCR cycler (BioMolecular Systems, USA). Each reaction was prepared in a final volume of 10 *µl* containing 2 *µl* of cDNA (25 ng/*µl*), 2 *µl* of Evagreen, 0.5 *µl* of forward primer (5'-CAAAGA-AAGGAGGTCAGGCAC-3', 5 *µM*), and 0.5 *µl* of reverse primer (5'-TGGTGATAGATGCCAGGT TTCT-3', 5 *µM*). To validate the PCR results, each genotype was sequenced using the HRM technique [33].

qRT-PCR was performed for 45 cycles with the following temperature conditions: 15 *min* of preincubation at 95°*C*, 15 *s* of denaturation at 95°*C*, 20 *s* of annealing at 60°*C*, 20 *s* of extension at 72°*C*, followed by a melting curve analysis conducted from 60°*C* to 95°*C*. HRM analysis was performed using the data derived from the melting curves by the Mic's qPCR analysis software [34].

Statistical analysis

Data analysis was performed using GraphPad Prism software (version 9.5.1, GraphPad software, San Diego, CA). Odds Ratios (ORs) with 95% Confidence intervals (Cis) were calculated to evaluate risk, and a p-value <0.05 was considered statistically significant. Group differences were assessed using the chi-square test.

Results

Scinderin protein profiling and retrieval of SNP data

The *SCIN* gene in humans consists of 89,463 base pairs, with its corresponding protein composed of 715 amino acids. An investigation into the presence of distinct functional domains within the SCIN protein-such as gelsolin_S1_like (10-121), VILL_6 (135-227), gelsolin_S3_like (246-346), gelsolin_S4_like (390-486), gelsolin_S5_like (508-598), and gelsolin_S6_like (613-711)-was conducted using resources from the InterPro and UniProtKB databases.

The structural data derived from the UniProtKB archive revealed specific domains that encompassed an actin-severing segment (1-363) and a Ca2+-dependent actin-binding region (364-715).

The RaptorX server predicted 18% α-helix, 28% β-sheet, and 53% coil for the SCIN protein. Additionally, three categories of residue-specific solvent accessibility were identified: exposed (40%), medium (33%), and buried (26%), Furthermore, 38 residues (5%) were predicted to be disordered. A total of 38,785 SNPs associated with the SCIN protein were retrieved from the dbSNP database, considering only nonredundant entries. The identified SNPs were assigned to distinct functional categories, including in-frame deletion [8], in-frame indel [2], in-frame insertion (3), start codon variant [7], intron (33343), missense (1054), noncoding transcript variant (6059), and synonymous (417) SNPs. The majority of SNPs were found within intronic regions, subsequently by noncoding transcript variants and nsSNPs. The distribution of these SNPs is shown in figure 2.

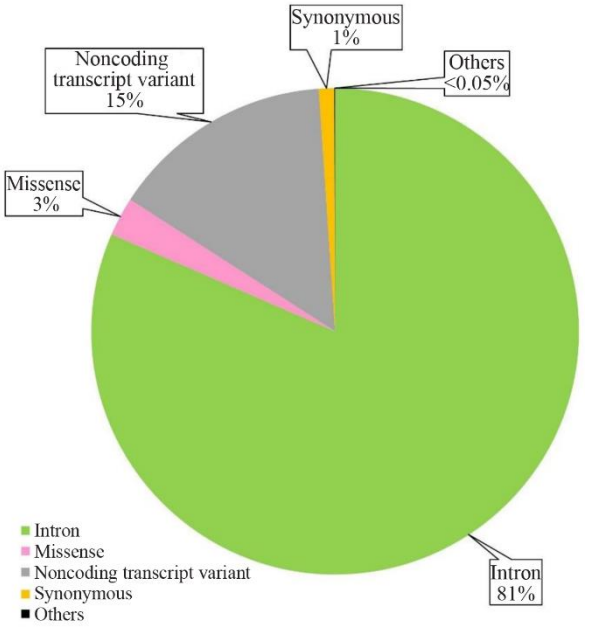

Figure 2. A graphical representation in the form of a pie chart illustrating the distribution of Single Nucleotide Polymorphisms (SNPs) within the *SCIN* gene, as sourced from the dbSNP database.

Identification of potentially deleterious SNP variants

To predict the pathogenicity or deleterious effects of nsSNPs, five bioinformatics tools—PolyPhen-2, SNAP2, Align GVGD, SIFT, and PANTHER—were utilized, each applied according to its respective predefined criteria. Consequently, 11 nsSNPs out of 1,054 were unanimously predicted to be deleterious by all five tools. When analyzed by PredictSNP, 9 mutations were classified as severely deleterious (Table 1).

Assessment of structural stability alterations in mutant proteins

MUpro and I-Mutant2.0 assessed the influence of various nsSNPs on the stability of the SCIN protein. The results indicated a general decrease in stability across all nsSNPs, except for the P382L SNP, which was predicted to enhance stability based on analysis conducted using IMutant2.0 (Table 2).

Prediction of structural effect of deleterious SNPs

Predictions generated by MutPred suggested potential gains of acetylation, modifications in metal binding, acquisition of catalytic sites, loss of ADP-ribosylation, and potential gains of phosphorylation. These predictions were accompanied by p-values and probability scores. A MutPred2 score, derived from machine-learning neural network algorithms, was also reported. This score estimates the likelihood of structural and functional changes, including intrinsic disorder, disruptions in ordered interfaces, metal binding, and helix modification. The score varies between 0 and 1, with a higher value indicating a greater probability that SNP-induced changes contribute to disease-related molecular mechanisms.

Table 1. Identification of deleterious Single Nucleotide Polymorphisms in the SCIN protein using various online prediction tools

SNP ID	AAS[1]	SIFT	SNP2	PANTHER	GVGD	PolyPhen-2	PredictSNP
rs370935948	T131R	Deleterious	Effect	Probably damaging	Class C65	Probably damaging	Deleterious
rs144832211	R145L	Deleterious	Effect	Probably damaging	Class C65	Probably damaging	Deleterious
rs189312864	R146G	Deleterious	Effect	Probably damaging	Class C65	Probably damaging	Deleterious
rs373419530	P271S	Deleterious	Effect	Probably damaging	Class C65	Probably damaging	Neutral
rs370586675	R306S	Deleterious	Effect	Probably damaging	Class C65	Probably damaging	Deleterious
rs372057101	P382L	Deleterious	Effect	Probably damaging	Class C65	Possibly damaging	Deleterious
rs199716870	M384T	Deleterious	Effect	Probably damaging	Class C65	Probably damaging	Neutral
rs370679250	W440R	Deleterious	Effect	Probably damaging	Class C65	Probably damaging	Deleterious
rs186847510	I492S	Deleterious	Effect	Probably damaging	Class C65	Probably damaging	Deleterious
rs376349889	R511G	Deleterious	Effect	Probably damaging	Class C65	Probably damaging	Deleterious
rs200503401	S620Y	Deleterious	Effect	Probably damaging	Class C65	Probably damaging	Deleterious

AAS[1]: Amino Acid Substitution

Table 2. Predictions of protein stability changes using I-Mutant 2.0 and MUpro.

SNP ID	AAS[1]	I-MUTANT2.0		MuPro	
		Stability	RI[2]	Stability	ΔG
rs370935948	T131R	Decrease	4	Decrease	-0.61
rs144832211	R145L	Decrease	8	Decrease	-0.3
rs189312864	R146G	Decrease	9	Decrease	-1.58
rs373419530	P271S	Decrease	9	Decrease	-1.04
rs370586675	R306S	Decrease	8	Decrease	-1.01
rs372057101	P382L	Increase	5	Decrease	-0.3
rs199716870	M384T	Decrease	7	Decrease	-0.89
rs370679250	W440R	Decrease	8	Decrease	-1.11
rs186847510	I492S	Decrease	7	Decrease	-1.87
rs376349889	R511G	Decrease	8	Decrease	-1.3
rs200503401	S620Y	Decrease	1	Decrease	-0.37

AAS[1]: Amino Acid Substitution, RI[2]: Reliability Index

As a result, all selected nsSNPs were considered highly plausible hypotheses, except for the T131R, R271T, and P382L mutations, which were classified as confident hypotheses (Table 3).

Computational analysis of nsSNP-induced changes in protein stability and interactions

The solvent accessibility of the SCIN protein was evaluated using the NetSurfP online tool. Notable transitions between exposed and buried states were observed. The results revealed that the M384T variant caused a transition from a buried to an exposed state, while the P382L variant resulted in a shift from an exposed to a buried state. Additionally, other mutations resulted in alterations in Relative Solvent Accessibility (RSA) and Absolute Solvent Accessibility (ASA) values, suggesting changes in solvent exposure (Table 4).

The mutations were further analyzed using the HOPE tool. The results showed that, among the seven mutations with a MetaRNN score exceeding 0.5, the score of five reflected modifications in the size of the amino acid, four indicated an alteration in charge, and six affected hydrophobicity. Additionally, various other biochemical properties were influenced by amino acid substitutions. According to the HOPE prediction report, the rs376349889 variant, which involves a glycine substitution (R511G), was particularly noteworthy. This substitution introduced flexibility due to glycine's structural properties, potentially disrupting the necessary rigidity at that specific position within the protein. Moreover, compared to the wild-type residue, the mutant residue was reduced in size. The mutant residue was neutral and showed increased hydrophobicity compared to the positively charged wild-type residue. Furthermore, the wild-type residue formed a salt bridge with residue number 527 (glutamic acid), which could be disturbed by the charge difference introduced by the mutant residue. The site of the mutation falls within a segment of residues identified in UniProt as a specialized region responsible for Ca^{2+}-dependent actin binding. Alterations in amino acid properties could potentially interfere with this region and impact its functionality (Table 5).

Structural analyses of protein mutations

Due to the absence of a full-length SCIN protein 3D structure in the Protein Data Bank (PDB), the FASTA-formatted amino acid sequence, along with mutated variants, was uploaded to the trRosetta server to generate 3D models of the SCIN protein (Figure 3A). Simi-

Table 3. Prediction of the functional and structural alterations using the MutPred2 server.

SNP	AAS[1]	MutPred2	
		Score	Molecular mechanisms
rs370935948	T131R	0.444	-
rs144832211	R145L	0.741	- Modified metal-binding capability - Modified DNA-binding affinity
rs189312864	R146G	0.754	- Modified metal-binding capability - Modified DNA-binding affinity - Altered Stability
rs373419530	P271T	0.35	-
rs370586675	R306S	0.866	- Altered Coiled coil - Changes in the ordered protein-protein interface - Acquisition of Acetylation at K307 - Acquisition of Ubiquitylation at K307 - Modified DNA-binding affinity - Transmembrane domain alteration - Elimination of GPI-anchor amidation at N302
rs372057101	P382L	0.189	-
rs199716870	M384T	0.583	- Gain of Intrinsic disorder - Phosphorylation site emerged at S381 - Transmembrane domain alteration
rs370679250	W440R	0.967	- Changes in the ordered protein-protein interface - Loop deletion - Acquisition of Relative solvent accessibility - Modified metal-binding capability - Acquisition of Catalytic site at W440 - Transmembrane domain alteration - Gain of N-linked glycosylation at N444
rs186847510	I492S	0.878	- Altered Stability - Acquisition of intrinsic disorder - Newly acquired Relative solvent accessibility - Newly acquired Acetylation at K495 - Transmembrane domain alteration - Newly acquired N-linked glycosylation at N496
rs376349889	R511G	0.84	- Gain of Strand - Transmembrane domain alteration - Elimination of ADP-ribosylation at R511
rs200503401	S620Y	0.805	- Newly acquired N-linked glycosylation at N621

AAS[1]: Amino Acid Substitution

Table 4. Structural evaluations of deleterious SCIN protein variants using the NetSurfP.2 web server

SNP ID	AAS[1]	NetSurfP.2					
		Wild class			Mutant class		
		RSA[2]	ASA[3] (A°)	Class alignment	Class alignment	RSA	ASA (A°)
rs370935948	T131R	0.53	72.826	Exposed	Exposed	0.55	126.85
rs144832211	R145L	0.61	140.32	Exposed	Exposed	0.28	51.4
rs189312864	R146G	0.5	114.21	Exposed	Exposed	0.5	35.3
rs373419530	P271S	0.34	48.88	Exposed	Exposed	0.46	53.54
rs370586675	R306S	0.21	49.6	Buried	Buried	0.16	18.94
rs372057101	P382L	0.57	80.37	Exposed	Buried	0.2	37.2
rs199716870	M384T	0.18	36.85	Buried	Exposed	0.31	42.36
rs370679250	W440R	0.03	6.4	Buried	Buried	0.08	18
rs186847510	I492S	0.07	13.11	Buried	Buried	0.16	18.99
rs376349889	R511G	0.16	36.41	Buried	Buried	0.04	2.87
rs200503401	S620Y	0.11	12.4	Buried	Buried	0.22	47.18

AAS[1]: Amino Acid Substitution, RSA[2]: Relative Solvent Accessibility, ASA[3]: Absolute Solvent Accessibility

Table 5. Analysis of structural impacts of the selected mutations using the Project HOPE web server

SNP ID	AAS[1]	HOPE				
		Size	Charge	HP[4]	MetaRNN score	Contacts
rs370935948	T131R	M[2]>W[3]	0 → +	↓	0.66	In the wild-type protein, the residue establishes a hydrogen bond with Asparagine at position 132. The substitution introduces a residue with a different size, preventing proper alignment necessary for this interaction. Furthermore, the altered hydrophobic properties of the mutant residue negatively influence the ability to form this hydrogen bond.
rs144832211	R145L	M<W	+ → 0	↑	0.1	In the wild-type protein, the residue forms a salt bridge with Glutamic Acid at position 186. However, a change in charge caused by the mutation disrupts this ionic interaction established by the original residue.
rs189312864	R146G	M<W	+ → 0	↑	0.06	Glycine's high flexibility may compromise the necessary structural rigidity of the protein at this site.
rs373419530	P271S	M<W	−	↓	0.85	-
rs370586675	R306S	M<W	+ → 0	↑	0.9	-
rs372057101	P382L	M>W	−	−	0.18	Proline is characterized by its rigidity, often imposing a unique backbone conformation that may be essential at this site. The mutation could disrupt this specific structural arrangement.
rs199716870	M384T	M<W	−	↓	0.6	In the wild-type protein, the residue forms a hydrogen bond with Aspartic Acid at position 374. Due to differences in size, the mutant residue does not properly align to maintain this interaction. Additionally, changes in hydrophobicity between the residues further disrupt the formation of the hydrogen bond.
rs370679250	W440R	M<W	0 → +	↓	0.99	-
rs186847510	I492S	M<W	−	↓	0.26	-
rs376349889	R511G	M<W	+ → 0	↑	0.92	In the wild-type protein, the residue establishes a salt bridge with Glutamic Acid at position 527. A change in charge caused by the mutation disrupts this ionic interaction formed by the original residue.
rs200503401	S620Y	M>W	−	−	0.54	In the wild-type protein, the residue forms a hydrogen bond with Glutamic Acid at position 666. However, due to the size difference, the mutant residue does not occupy the correct position to maintain this interaction.

AAS[1]: Amino Acid Substitution, M[2]: Mutant, W[3]: Wild, HP[4]: Hydrophobicity.

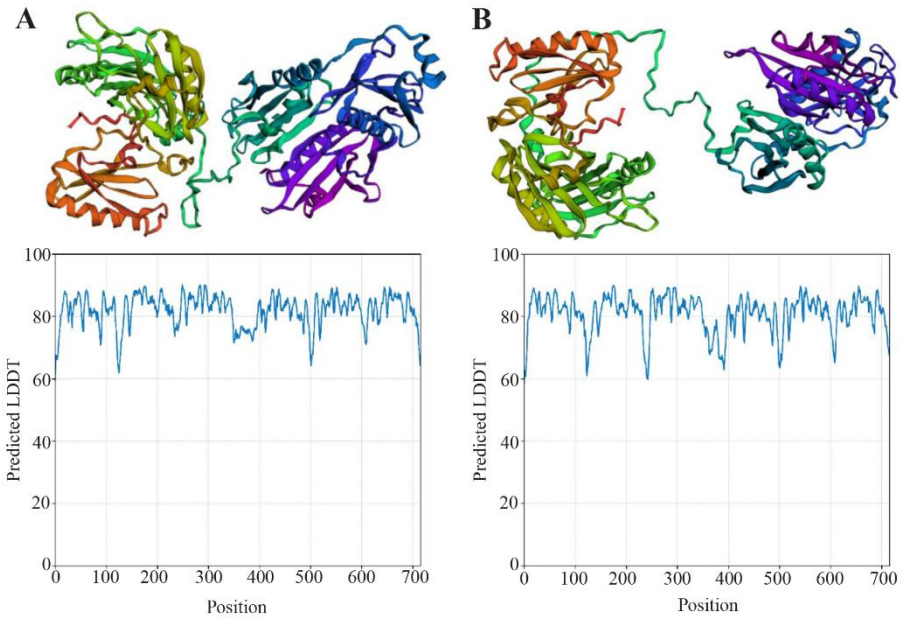

Figure 3. 3D Protein Modeling and Quality assessment of SCIN proteins using trRosetta. A) Wild-type SCIN, B) R511G mutant. Comparison of predicted local confidence (pLDDT) scores for the wild-type (A) and mutant (B) proteins, showing overall similar structural reliability with minor local variations.

larly, the same procedure was applied to generate a model for the mutated protein (Figure 3B). The predicted wild-type and mutant protein models had Template Modeling (TM) scores of 0.710 and 0.706, respectively. A TM-score greated than 0.5 indicates considerable similarity in three-dimensional conformation between the predicted protein models and their template structures. Both models demonstrated TM-scores above 0.5, suggesting reliable structural predictions.

The degree of structural similarity between the native and mutant models was assessed using TM-score and RMSD values *via* the TM-align tool (Figure 4). The predicted mutant model obtained a TM score of 0.48, suggesting notable structural divergence from the wild-type protein. Additionally, RMSD analysis was conducted to quantify structural deviations in the mutant model relative to the wild-type protein, revealing a value of 6.24, indicating considerable structural instability associated with this high-risk nsSNP.

Prediction of mutation-induced structural and stability changes using DynaMut

The impact of the mutation on protein stability and dynamics was assessed using the DynaMut web server. The ΔΔG values obtained from different prediction algorithms indicated a generally destabilizing effect. Specifically, the overall DynaMut ΔΔG was –0.068 *kcal/mol*, while ENCoM (–0.080 *kcal/mol*), mCSM (–1.451 *kcal/mol*), and DUET (–1.116 *kcal/mol*) consistently predicted destabilization. In contrast, the SDM method suggested a slight stabilizing effect with a ΔΔG of +0.370 *kcal/mol*. Additionally, the change in vibrational entropy energy (ΔΔSVib ENCoM=+0.100 *kcal/mol*·K) revealed an increase in molecular flexibility in the mutant structure compared to the wild type. To further investigate the destabilizing effects of the mutation, an interatomic interaction analysis was conducted. To further investigate the destabilizing effects of the mutation, an interatomic interaction analysis was conducted. The wild-type residue (green) formed multiple stabilizing interactions, including ionic interactions and hydrogen bonds, whereas the mutant residue showed reduced bonding interactions, indicating decreased local stability (Figure 5).

Analysis of gene-gene and protein-protein interactions

The GeneMANIA tool was utilized to evaluate gene-gene interactions involving the SCIN protein, revealing an association with the *TMOD2* gene. Additionally, figure 6 illustrates the co-expressed genes and their roles in achieving similar functions or sharing common protein domains. The investigation revealed interactions between the SCIN protein and several proteins involved in cytoskeletal functions, including HCLS1 (Hematopoietic Lineage Cell-Specific Lyn Substrate 1), CTTN (Src substrate cortactin), TLN1 (Talin-1), WASL (Neural Wiskott-Aldrich syndrome), and TLN2 (Talin-2). Additional protein interactions are depicted in figure 7.

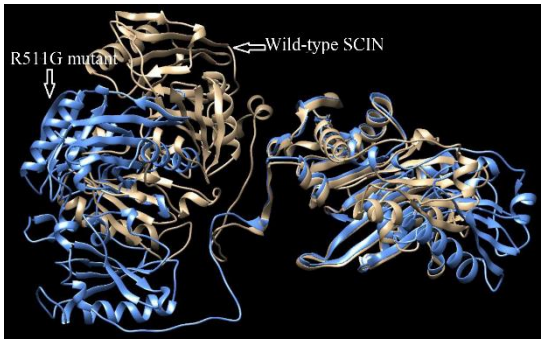

Figure 4. Superimposed structure of Wild-type SCIN and its R511G mutant generated by the TM-align tool. High RMSD (6.24) and low TM score values (0.48) indicate structural dissimilarity due to R511G mutation. The Wild-type structure is shown in gold, while the R511G mutant is shown in blue.

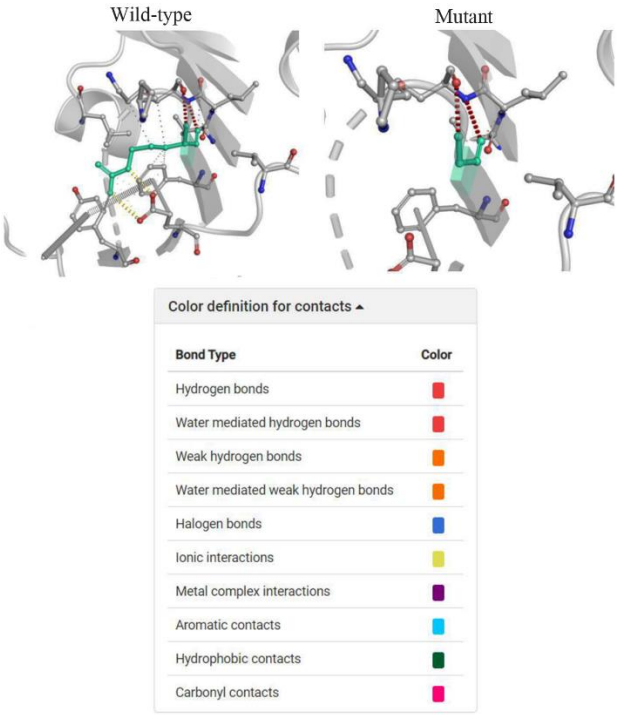

Figure 5. Comparative structural analysis of the mutant (R511G) SCIN protein in comparison to the wild-type structure generated by DynaMut. In the wild-type conformation, the residue of interest (green) establishes multiple stabilizing contacts, including ionic interactions, aromatic contacts and hydrogen bonds, whereas the mutant conformation exhibits a marked reduction in these interactions, suggesting decreased local stability and potential structural rearrangements.

Analysis of HRM results

We examined the rs376349889 (C>G) variant in-both gastric and colorectal cancer samples, utilizing genotypic data obtained from the HRM test. Genotyping was conducted on 200 patients diagnosed with CRC and 200 patients diagnosed with GC (both female and male), focusing on the rs376349889 variant. The allele frequencies and genotype distributions for each

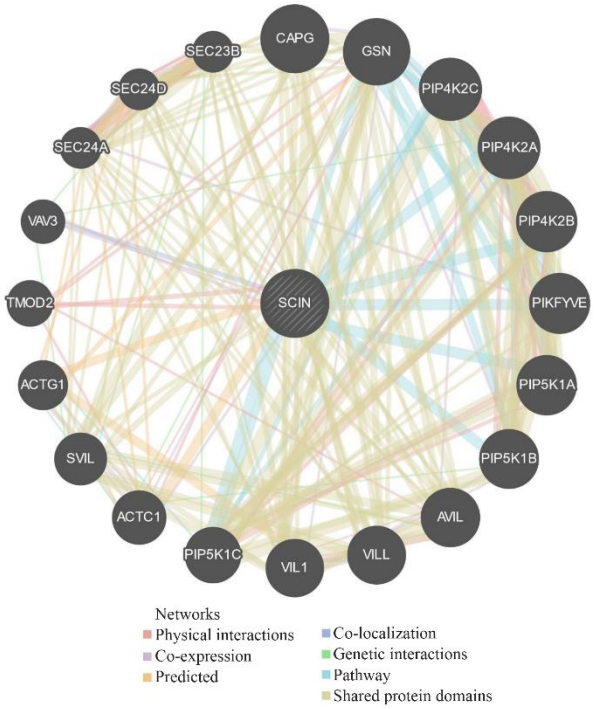

Figure 6. GeneMANIA-based analysis of SCIN *SCIN* gene interactions.

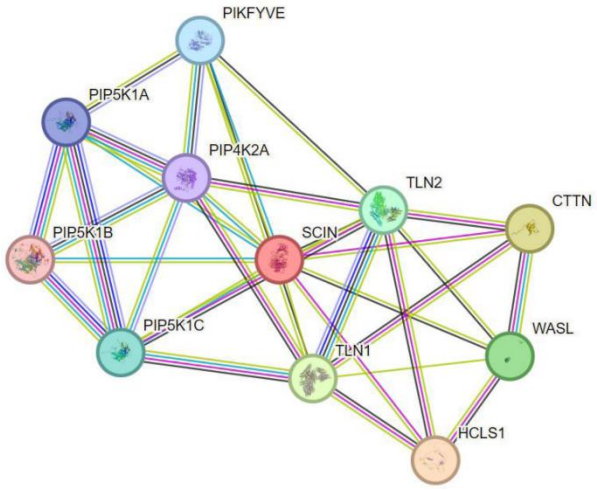

Figure 7. SCIN protein interaction network constructed *via* STRING.

group are summarized in table 6. A marked difference in rs376349889 frequency was observed among GC patients, CRC patients, and the control group. The primary element that differentiates wild type (CC), homozygous (GG), and heterozygous (GC) genotypes is the variation in melting temperature and TM point, as illustrated in figure 8. Analysis revealed that the G allele was more prevalent in GC samples compared to the wild-type C allele. Additionally, the GG genotype was more common in gastric cancer samples than the CC genotype when compared to healthy control samples. Comparable patterns were also detected in CRC samples (Table 6).

Discussion

Global cancer statistics from 2022 indicate that approximately 20 million new cancer cases were diagnosed, resulting in nearly 10 million deaths attributed to the disease. Projections for 2050 forecast an annual incidence of 35 million new cancer cases, reflecting a 77% increase from 2022 figures [35]. Notably, gastrointestinal cancers, including gastric and CRC, are significant contributors to cancer-related mortality [36].

Scinderin, an actin-binding and actin-severing protein, is essential for the regulation of cytoskeletal dynamics [7]. Several studies have reported altered *SCIN* expression in various cancer types, suggesting its potential involvement in tumorigenesis, acting as either a

Table 6. Frequency of rs376349889 genotypes, allelic frequencies and genotype distribution in Gastric Cancer (GC) and Colorectal Cancer (CRC) patients compared with control subjects

Frequency of rs376349889 genotypes				Allelic frequencies and genotype distribution				
Cancer type	Genotypes	Group		Genotype	OR	CI		p-value
		Control	Tumor			Lower	Upper	
Gastric cancer								
	CC	94 (47%)	37 (18.5%)	*G/C*	2.825	2.119	3.766	<0.0001
	CG	77 (38.5%)	90 (45%)	*GG+GC/CC*	3.907	2.486	6.14	<0.0001
	GG	29 (14.5%)	73 (36.5%)	*GG/GC+CC*	0.097	0.06	0.159	<0.0001
	Total	200 (100%)	200 (100%)	*GC/GG+CC*	1.307	0.877	1.947	0.187
Colorectal cancer								
	CC	94 (47%)	56 (28%)	*G/C*	1.924	1.447	2.559	<0.0001
	CG	77 (38.5%)	90 (45%)	*GG+GC/CC*	2.28	1.506	3.454	<0.0001
	GG	29 (14.5%)	54 (27%)	*GG/GC+CC*	2.181	1.32	3.604	0.002
	Total	200 (100%)	200 (100%)	*GC/GG+CC*	1.307	0.877	1.947	0.223

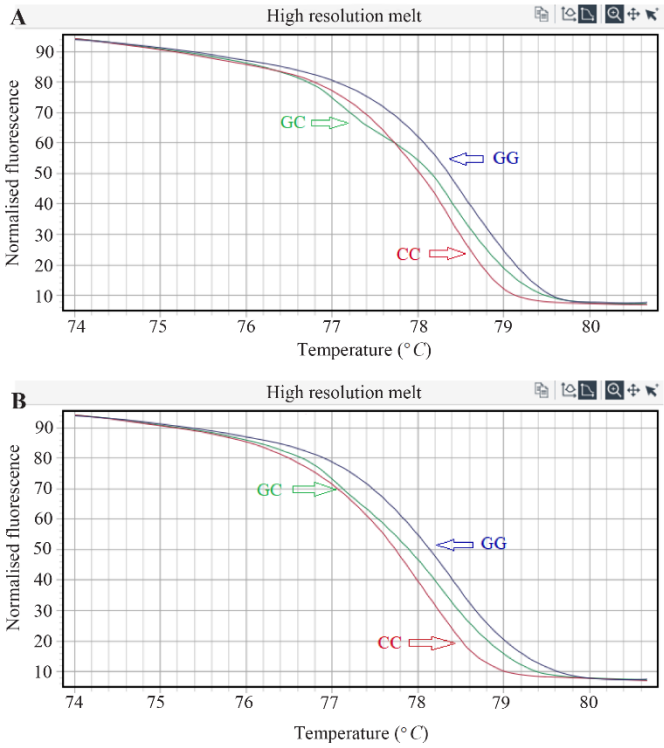

Figure 8. The distinction in melting profiles among wild type (CC), homozygous (GG), and heterozygous (GC) genotypes; (A) gastric cancer patients, (B) colorectal cancer patients.

tumor suppressor or an oncogene depending on the tissue. Current evidence is limited and sometimes conflicting, with studies reporting both increased and decreased expression associated with malignancy [37-39]. In megakaryoblastic leukemia, ectopic expression of SCIN reorganizes actin filaments *via* Rho GTPases (CDC42, Rac1), leading to differentiation, maturation, and apoptosis with release of platelet-like particles. These effects are accompanied by suppression of proliferation and tumorigenesis, partly through modulation of PI3K/AKT and MAPK/ERK signaling pathways [40]. These findings underscore the complexity of SCIN's function in tumorigenesis. Further research is needed to clarify its molecular mechanisms and evaluate its potential as a context-specific prognostic marker or therapeutic target.

In this study, nsSNPs were analyzed using six computational tools: SIFT, PANTHER, PolyPhen-2, SNAP2, PredictSNP, and Align-GVGD. This approach aimed to leverage their diverse predictive capabilities and improve filtration accuracy. SIFT classifies substitutions based on evolutionary conservation, with scores ≤0.05 considered deleterious [17]. PolyPhen-2 integrates evolutionary, structural, and physicochemical features, where variants labeled probably damaging are more likely to impair protein function [18]. PANTHER uses evolutionary conservation, with subPSEC scores ≤−3 indicating a higher likelihood of deleterious impact [19]. SNAP2 employs neural network-based integration of sequence, structural, and physicochemical features, where positive scores suggest deleterious effects and negative scores indicate tolerated variants [20]. Align-GVGD combines evolutionary conservation and amino acid chemical differences, classifying variants from C0 to C65, with higher classes reflecting greater likelihood of deleterious impact [21]. PredictSNP provides a consensus prediction by integrating multiple tools, where variants classified as deleterious with high confidence are more likely to disrupt protein function [22], Due to the unique parameters of each algorithm, nine nsSNPs were consistently classified as highly deleterious across all tools, warranting further investigation (Table 1).

Protein stability is essential for maintaining proper molecular function. Missense mutations can impair a polypeptide's ability to adopt the correct functional conformation, leading to decreased stability. Consequently, mutant proteins are more susceptible to misfolding, aggregation, or degradation. Reduced stability and misfolding are significant outcomes of damaging missense variants [41].

To assess the impact of nsSNPs on protein stability, we utilized the MUpro and I-Mutant3.0 online tools for both wild-type and mutant SCIN proteins (Table 2). These tools estimate whether amino acid substitutions increase or decrease stability, reporting complementary outputs: MUpro provides scores ranging from -1 to +1, while I-Mutant 3.0 calculates ΔΔG values (*kcal/mol*) along with a reliability index (RI) [23,24]. The thermodynamic stability of a protein is indicated by the Gibbs free energy of folding (ΔG), which represents the energy difference between its folded and unfolded forms. When ΔΔG is positive, it implies greater stability; conversely, a negative ΔΔG indicates reduced stability [42]. Our analysis showed that most nsSNPs within the *SCIN* gene decreased protein stability, except for the P382L variant, which was predicted to enhance stability by I-Mutant2.0.

MutPred2 was employed to evaluate the functional consequences of amino acid substitutions based on physicochemical properties such as ubiquitylation, methylation, acetylation, and changes in ordered/ disordered interfaces, generating a general deleteriousness score from 0 to 1, where scores >0.5 indicate a higher likelihood of pathogenicity [25]. Six nsSNPs were predicted to induce significant structural and functional alterations, each scoring above 0.75 on the severity scale (Table 3).

Beyond functional predictions, assessing structural properties such as solvent accessibility, secondary structure, and structural disorder provides additional insights into the potential impacts of these variants. Using NetSurfP-2.0, provided insights into the secondary structure (H: helix, E: strand, C: coil), RSA, 0–1 and ASA, disorder probability (0–1, with values near 1 indicating disordered regions), and backbone dihedral angles (φ, ψ) of each amino acid, enabling detailed

structural analysis [26]. Among the 11 highly deleterious nsSNPs, the M384T mutation was identified as surface-exposed, while P382L was buried. Four mutations (T131R, R145L, and R146G) were located on the protein surface, potentially affecting the physiological properties of the protein, such as stability, charge distribution, and accessible surface area. Conversely, five buried nsSNPs (K306S, W440R, I492S, R511G, and S620Y) may disrupt protein folding and function (Table 4).

Structural assessment using the HOPE server revealed hydrophobicity, charge, and size variations between the wild-type and mutant amino acids, potential effects on protein structure and stability, visualizations and 3D models when structural data are available, and a summary of the likely impact on protein function [27]. Seven substitutions—T131R, P271S, R306S, M384T, W440R, R511G, and S620Y—had a MetaRNN score of ≥0.5, indicating potential pathogenicity. Notably, W440R and R511G had scores exceeding 0.9, suggesting a high likelihood of functional disruption. For instance, rs376349889 results in the substitution of arginine (R) with glycine (G) at position 511. Glycine, being smaller and uncharged, differs significantly from the positively charged wild-type arginine, affecting local hydrophobicity and disrupting hydrogen bonding. In addition, a salt bridge is formed between arginine and glutamic acid at position 527—an interaction lost in the mutant protein—which may affect the actin-binding capacity of the SCIN protein (Table 5).

While residue-level analyses highlight local disruptions, investigating the impact on overall protein architecture required structural modeling. Due to the lack of a comprehensive structural model for the human SCIN protein (715 amino acids) in the Protein Data Bank, computational modeling was performed using trRosetta, which provided outputs including pairwise distance maps between all residues, predicted backbone dihedral angles (φ, ψ, ω), 3D protein models in PDB format, and quality scores indicating the confidence of the structural predictions [28]. The wild-type and R511G mutant models had TM-scores of 0.710 and 0.706, respectively, as calculated by trRosetta —both values above 0.5, indicating reliable topological similarity (Figure 3) TM-align compared 3D protein structures using TM-scores, RMSD, and residue-level alignments to assess changes induced by nsSNPs, revealed a significant conformational shift in the R511G variant, evidenced by an RMSD value of 6.24 and a decreased TM score of 0.484 (Figure 4). High RMSD values (typically >2–3 Å) indicate low structural similarity, suggesting significant conformational differences that may affect protein function. In contrast, TM-scores values below the 0.5 threshold, the topological similarity is considered unreliable, suggesting that the mutation may alter the overall fold or conformation of the protein and thereby compromise its function [29].

The computational analysis by DynaMut indicated that the mutation leads to modest but consistent destabilization of the protein structure, as supported by mCSM and DUET, while SDM predictions diverged due to its reliance on sequence-based rather than structural information. Although ΔΔG values from DynaMut and ENCoM (–0.068 and –0.080 *kcal/mol*) were close to the neutral threshold (–0.5 to +0.5 *kcal/mol*) [43], the more negative values from mCSM (–1.451 *kcal/mol*) and DUET (–1.116 *kcal/mol*) support a destabilizing effect. The positive ΔΔSVib further suggests increased molecular flexibility and reduced conformational stability. Such changes in dynamic behavior may weaken intramolecular interactions, thereby affecting the protein's overall structural integrity and potentially altering its functional properties. Structural comparison revealed that, unlike the wild-type residue which formed stabilizing hydrogen and ionic bonds, the mutant residue showed a loss of these interactions and aromatic contacts, indicating weakened local stability and possible structural rearrangements that may compromise protein function. Gene interaction analysis revealed a strong association between the *SCIN* gene and various members of the GSN gene family. Prior research efforts have revealed that *TMOD2* is considerably overexpressed in cells isolated from breast and prostate carcinomas [44,45]. In colorectal cancer, *VAV3* has been linked to increased tumor invasion and metastasis [46], while *AVIL* overexpression in glioblastoma stimulates cell proliferation and migration [47]. Additionally, *SVIL* is implicated in gastric cancer progression but is downregulated in bladder cancer [48]. These findings suggest that deleterious SNPs within the *SCIN* gene could affect broader gene networks (Figure 6). Network analysis using GeneMANIA further highlighted potential functional interactions between *SCIN* and these cancer-associated genes, providing insight into how deleterious nsSNPs might perturb key oncogenic and tumor-suppressive pathways.

Beyond SCIN, the analyzed signaling network includes both oncogenes and tumor suppressors. PIP5K1A, CTTN and TLN1 act as oncogenes, promoting tumor progression and metastasis [49-51]. Conversely, PIP4K2A, TLN2, WASL, and HCLS1 function as tumor suppressors, regulating PI3K and Wnt/β-catenin signaling, cytoskeletal dynamics, or anti-tumor immunity [52-55]. PIKFYVE additionally modulates tumor immunity by enhancing MHC class I surface expression, offering a potential therapeutic target [56]. Although the roles of PIP5K1B, PIP5K1C, and TLN1 are less defined, integrating these proteins with SCIN variants highlights the complex network influencing cancer progression and may guide future therapeutic strategies (Figure 7).

Having identified *SCIN*'s potential interaction network, we further investigated the clinical significance of specific *SCIN* variants. Genotypic analysis of rs376349889 (C/G) in gastric and colorectal cancer

samples revealed significant associations between the GG genotype and increased disease risk. OR calculations indicated that allele G increases the likelihood of cancer by 2.825 times (GC) and 1.924 times (CRC), further supporting its pathogenic potential (Table 6).

Although SCIN has emerging roles in cytoskeletal regulation and tumor-related processes, there is still very little population-based genetic evidence directly linking *SCIN* variants to human disease. Thus far, the only published document comes from a melanoma epistasis study, where an intronic *SCIN* polymorphism (rs7798406) showed a significant interaction with a CDC42 variant (rs3117048) in influencing Breslow thickness [57]. Apart from this finding, genome-wide association studies have not identified *SCIN* as a locus of major effect, highlighting the need for more comprehensive genetic and functional studies to better define the role of *SCIN* variants in cancer development and progression. Given the scarcity of current data, it is still uncertain whether *SCIN* polymorphisms independently affect cancer risk and prognosis, or whether their influence is conditional and mediated through interactions with other signaling networks.

Conclusion

This research highlights the impact of single nucleotide polymorphisms in the *SCIN* gene, notably R511G, on protein stability and their possible involvement in cancer progression. These substitutions may disrupt the cell's internal structure, potentially promoting tumor growth in gastrointestinal cancers. While present findings strongly suggest a connection, experimental validation through laboratory studies is necessary to validate these effects. Additionally, further research should investigate how these substitutions influence the behavior and function of cancer cells. Large-scale genetic studies could also help determine whether *SCIN* substitutions are reliable biomarkers, facilitating earlier detection and more targeted treatments for individuals at risk.

Acknowledgement

We would like to thank the University of Mazandaran's Research Department.

Conflict of Interest

The authors declare no conflict of interest.

References

1. Smyth EC, Nilsson M, Grabsch HI, van Grieken NC, Lordick F. Gastric cancer. Lancet 2020;396(10251):635-648.
2. Sung H, Ferlay J, Siegel RL, Laversanne M, Soerjomataram I, Jemal A, et al. Global cancer statistics 2020: GLOBOCAN estimates of incidence and mortality worldwide for 36 cancers in 185 countries. CA Cancer J Clin 2021;71(3):209-249.
3. Yuen ST, Leung SY. Genomics study of gastric cancer and its molecular subtypes. Stem Cells, Pre-neoplasia, and Early Cancer of the Upper Gastrointestinal Tract. 2016 Aug 30:419-39.
4. Siegel RL, Wagle NS, Cercek A, Smith RA, Jemal A. Colorectal cancer statistics, 2023. CA Cancer J Clin 2023;73(3):233-254.
5. Sawicki T, Ruszkowska M, Danielewicz A, Niedźwiedzka E, Arłukowicz T, Przybyłowicz KE. A review of colorectal cancer in terms of epidemiology, risk factors, development, symptoms and diagnosis. Cancers (Basel) 2021;13(9):2025.
6. Keum N, Giovannucci EL. Epidemiology of colorectal cancer. InPathology and epidemiology of cancer 2016 Sep 2 (pp. 391-407). Cham: Springer International Publishing.
7. Trifaro J, Rose S, Marcu M. Scinderin, a Ca2+-dependent actin filament severing protein that controls cortical actin network dynamics during secretion. Neurochem Res 2000;25:133-144.
8. Chen XM, Guo JM, Chen P, Mao LG, Feng WY, Le DH, et al. Suppression of scinderin modulates epithelial-mesenchymal transition markers in highly metastatic gastric cancer cell line SGC-7901. Mol Med Rep 2014; 10(5):2327-233.
9. Trifaró JM, Gasman S, Gutierrez L. Cytoskeletal control of vesicle transport and exocytosis in chromaffin cells. Acta Physiol (Oxf) 2008;192(2):165-172.
10. Landau DA, Tausch E, Taylor-Weiner AN, Stewart C, Reiter JG, Bahlo J, et al. Mutations driving CLL and their evolution in progression and relapse. Nature 2015;526 (7574);525-530.
11. Liu J, He C, Xing C, Yuan Y. Nucleotide excision repair related gene polymorphisms and genetic susceptibility, chemotherapeutic sensitivity and prognosis of gastric cancer. Mutat Res 2014;765:11-21.
12. Oldridge DA, Wood AC, Weichert-Leahey N, Crimmins I, Sussman R, Winter C, et al. Genetic predisposition to neuroblastoma mediated by a LMO1 super-enhancer polymorphism. Nature 2015;528(7582):418-421.
13. Yang W, Zhang T, Song X, Dong G, Xu L, Jiang F. SNP-target genes interaction perturbing the cancer risk in the post-GWAS. Cancers (Basel) 2022;14(22):5636.
14. Blum M, Chang HY, Chuguransky S, Grego T, Kandasaamy S, Mitchell A, et al. The InterPro protein families and domains database: 20 years on. Nucleic Acids Res 2021;49(D1):D344-D354.
15. Wang S, Li W, Liu S, Xu J. RaptorX-Property: a web server for protein structure property prediction. Nucleic Acids Res 2016;44(W1):W430-W435.
16. Sherry ST, Ward MH, Kholodov M, Baker J, Phan L, Smigielski EM, et al. dbSNP: the NCBI database of genetic variation. Nucleic Acids Res 2001;29(1):308-311.
17. Vaser R, Adusumalli S, Leng SN, Sikic M, Ng PC. SIFT missense predictions for genomes. Nat Protoc 2016;11 (1):1-9.

18. Adzhubei IA, Schmidt S, Peshkin L, Ramensky VE, Gerasimova A, Bork P, et al. A method and server for predicting damaging missense mutations.Nat Methods 2010;7(4):248-249.
19. Tang H, Thomas PD. PANTHER-PSEP: predicting disease-causing genetic variants using position-specific evolutionary preservation. Bioinformatics 2016;32(14): 2230-2232.
20. Hecht M, Bromberg Y, Rost B. Better prediction of functional effects for sequence variants. BMC Genomics 2015;16 Suppl 8(Suppl 8):S1.
21. Tavtigian SV, Deffenbaugh AM, Yin L, Judkins T, Scholl T, Samollow PB, et al. Comprehensive statistical study of 452 BRCA1 missense substitutions with classification of eight recurrent substitutions as neutral. J Med Genet 2006;43(4):295-305.
22. Bendl J, Stourac J, Salanda O, Pavelka A, Wieben ED, Zendulka J, et al. PredictSNP: robust and accurate consensus classifier for prediction of disease-related mutations. PLoS Comput Biol 2014;10(1):e1003440.
23. Capriotti E, Fariselli P, Casadio R. I-Mutant2. 0: predicting stability changes upon mutation from the protein sequence or structure. Nucleic Acids Res 2005;33 (suppl_2):W306-W310.
24. Cheng J, Randall A, Baldi P. Prediction of protein stability changes for single-site mutations using support vector machines. Proteins 2006;62(4):1125-1132.
25. Pejaver V, Urresti J, Lugo-Martinez J, Pagel KA, Lin GN, Nam HJ, et al. Inferring the molecular and phenotypic impact of amino acid variants with MutPred2. Nat Commun 2020; 11(1):5918.
26. Petersen B, Petersen TN, Andersen P, Nielsen M, Lundegaard C. A generic method for assignment of reliability scores applied to solvent accessibility predictions. BMC Struct Biol 2009;9(1):51.
27. Venselaar H, Te Beek TA, Kuipers RK, Hekkelman ML, Vriend G. Protein structure analysis of mutations causing inheritable diseases. An e-Science approach with life scientist friendly interfaces. BMC Bioinf 2010;11:548.
28. Yang J, Anishchenko I, Park H, Peng Z, Ovchinnikov S, Baker D. Improved protein structure prediction using predicted interresidue orientations. Proc Natl Acad Sci USA 2020;117(3):1496-1503.
29. Zhang Y, Skolnick J. TM-align: a protein structure alignment algorithm based on the TM-score. Nucleic Acids Res 2005;33(7):2302-2309.
30. Rodrigues CH, Pires DE, Ascher DB. DynaMut: predicting the impact of mutations on protein conformation, flexibility and stability. Nucleic Acids Res 2018;46(W1): W350-W355.
31. Franz M, Rodriguez H, Lopes C, Zuberi K, Montojo J, Bader GD, et al. GeneMANIA update 2018. Nucleic Acids Res 2018;46(W1):W60-W64.
32. Szklarczyk D, Franceschini A, Wyder S, Forslund K, Heller D, Huerta-Cepas J, et al. STRING v10: protein–protein interaction networks, integrated over the tree of life. Nucleic Acids Res 2015;43(Database issue):D447-D452.
33. Reed GH, Kent JO, Wittwer CT. High-resolution DNA melting analysis for simple and efficient molecular diagnostics. Pharmacogenomics 2007;8(6):597-608.
34. Bio Molecular Systems. Mic qPCR Cycler User Manual. Queensland, Australia: Bio Molecular Systems; 2023
35. Bray F, Laversanne M, Sung H, Ferlay J, Siegel RL, Soerjomataram I, et al. Global cancer statistics 2022: GLOBOCAN estimates of incidence and mortality worldwide for 36 cancers in 185 countries. CA Cancer J Clin 2024;74(3):229-263.
36. Ferlay J, Soerjomataram I, Dikshit R, Eser S, Mathers C, Rebelo M, et al. Cancer incidence and mortality worldwide: sources, methods and major patterns in GLOBOCAN 2012. Int J Cancer 2015;136(5):E359-E386.
37. Liu H, Shi D, Liu T, Yu Z, Zhou C. Lentivirus-mediated silencing of SCIN inhibits proliferation of human lung carcinoma cells. Gene 2015;554(1):32-39.
38. Qiao X, Zhou Y, Xie W, Wang Y, Zhang Y, Tian T, et al. Scinderin is a novel transcriptional target of BRMS1 involved in regulation of hepatocellular carcinoma cell apoptosis. Am J Cancer Res 2018; 8(6):1008–1018.
39. Zhou B, Chen TW, Jiang YB, Wei XB, Lu CD, Li JJ, et al. Scinderin suppresses cell proliferation and predicts the poor prognosis of hepatocellular carcinoma. Oncol Lett 2020;19(3):2011-20.
40. Zunino R, Li Q, Rosé SD, Romero-Benítez MM, Lejen T, Brandan NC, et al. Expression of scinderin in megakaryoblastic leukemia cells induces differentiation, maturation, and apoptosis with release of plateletlike particles and inhibits proliferation and tumorigenesis. Blood 2001;98(7):2210-9.
41. Bross P, Corydon TJ, Andresen BS, Jørgensen MM, Bolund L, Gregersen N. Protein misfolding and degradation in genetic diseases. Hum Mutat 1999;14(3):186-198.
42. Ferrer-Costa C, Orozco M, de la Cruz X. Characterization of disease-associated single amino acid polymorphisms in terms of sequence and structure properties. J Mol Biol 2002;315(4):771-786.
43. Capriotti E, Fariselli P, Rossi I, Casadio R. A three-state prediction of single point mutations on protein stability changes. BMC Bioinformatics 2008;9(Suppl 2):S6.
44. Majed SO. RNA sequencing-based total RNA profiling; the oncogenic MiR-191 identification as a novel biomarker for breast cancer. Cell Mol Biol (Noisy-le-grand) 2022;68(1):177-191.
45. Peng Y, Dong S, Yang Z, Song Y, Ding J, Hou D, et al. Identification of docetaxel-related biomarkers for prostate cancer. Andrologia 2021;53(7):e14079.
46. Uen YH, Fang CL, Hseu YC, Shen PC, Yang HL, Wen KS, et al. VAV3 oncogene expression in colorectal cancer: clinical aspects and functional characterization. Sci Rep 2015;5(1):9360.
47. Xie Z, Janczyk, PŁ, Zhang Y, Liu A, Shi X, Singh S, et al. A cytoskeleton regulator AVIL drives tumorigenesis in glioblastoma. Nat Commun 2020;11(1):3457.
48. Nie Z, Guo N, Peng Y, Gao Y, Cao H, Zhang S. Duality of the SVIL expression in bladder cancer and its cor-

relation with immune infiltration. Sci Rep 2023;13(1): 14595.

49. Yin M, Wang Y. The role of PIP5K1A in cancer development and progression. Med Oncol 2022;39(10):151.
50. Luo ML, Wang MR. CTTN (EMS1): an oncogene contributing to the metastasis of esophageal squamous cell carcinoma. Cell Res 2007;17(4):298–300.
51. Li S, Chen A, Gui J, Zhou H, Zhu L, Mi Y. TLN1: an oncogene associated with tumorigenesis and progression. Discov Oncol 2024;15(1):716.
52. Shin YJ, Sa JK, Lee Y, Kim D, Kim J, Kim DH, et al. PIP4K2A as a negative regulator of PI3K in PTEN-deficient glioblastoma. J Exp Med 2019;216(5):1120–1134.
53. Cai J, Huang Z, Zhou J, Wu W, Ye Y. TLN2 functions as a tumor suppressor in clear cell renal cell carcinoma via inactivation of the Wnt/β-catenin signaling pathway. Transl Androl Urol 2022 Jan;11(1):39–52.
54. Schwickert A, Weghake E, Brüggemann K, Engbers A, Brinkmann BF, Kemper B, et al. microRNA miR-142-3p Inhibits Breast Cancer Cell Invasiveness by Synchronous Targeting of WASL, Integrin Alpha V, and Additional Cytoskeletal Elements. PLoS One 2015 Dec 10;10(12): e0143993.
55. Yang C, Yang J, Li H, Fan W, Wang J. Therapeutic efficacy of 5-alkylresorcinol on progression of colorectal cancer by activating HCLS1 and suppressing TLR4/MYD88/NF-κB signaling. Eur J Med Res 2025 Jun 18;30(1):487.
56. Bao Y, Qiao Y, Choi JE, Zhang Y, Mannan R, Cheng C, et al. Targeting the lipid kinase PIKfyve upregulates surface expression of MHC class I to augment cancer immunotherapy. Proc Natl Acad Sci USA 2023 Dec 5;120(49):e2314416120.
57. Vaysse A, Fang S, Brossard M, Wei Q, Chen WV, Mohamdi H, et al. A comprehensive genome-wide analysis of melanoma Breslow thickness identifies interaction between CDC42 and SCIN genetic variants. Int J Cancer. 2016 Nov 1;139(9):2012-20.